CrossMark

A Case Study of the Weather Research and Forecasting Model Applied to the Joint Urban 2003 Tracer Field Experiment. Part 2: Gas Tracer Dispersion

Matthew A. Nelson[1] · Michael J. Brown[1] · Scot A. Halverson[1] ·
Paul E. Bieringer[2] · Andrew Annunzio[3] · George Bieberbach[2] ·
Scott Meech[4]

Abstract The Quick Urban & Industrial Complex (QUIC) atmospheric transport, and dispersion modelling, system was evaluated against the Joint Urban 2003 tracer-gas measurements. This was done using the wind and turbulence fields computed by the Weather Research and Forecasting (WRF) model. We compare the simulated and observed plume transport when using WRF-model-simulated wind fields, and local on-site wind measurements. Degradation of the WRF-model-based plume simulations was cased by errors in the simulated wind direction, and limitations in reproducing the small-scale wind-field variability. We explore two methods for importing turbulence from the WRF model simulations into the QUIC system. The first method uses parametrized turbulence profiles computed from WRF-model-computed boundary-layer similarity parameters; and the second method directly imports turbulent kinetic energy from the WRF model. Using the WRF model's Mellor-Yamada-Janjic boundary-layer scheme, the parametrized turbulence profiles and the direct import of turbulent kinetic energy were found to overpredict and underpredict the observed turbulence quantities, respectively. Near-source building effects were found to propagate several km downwind. These building effects and the temporal/spatial variations in the observed wind field were often found to have a stronger influence over the lateral and vertical plume spread than the intensity of turbulence. Correcting the WRF model wind directions using a single observational location improved the performance of the WRF-model-based simulations, but

---

✉ Matthew A. Nelson
 nelsonm@lanl.gov

1 Los Alamos National Laboratory, PO Box 1663, MS F609, Los Alamos, NM 87545, USA

2 Aeris, 1314 Main Street, Suite 101, Louisville, CO 80027, USA

3 Citadel, 131 South Dearborn Street, Chicago, IL 60603, USA

4 Science and Technology in Atmospheric Research (STAR) LLC, 3125 Sterling Circle, Suite 107, Boulder, CO 80301, USA

using the spatially-varying flow fields generated from multiple observation profiles generally provided the best performance.

1 Introduction

The Quick Urban & Industrial Complex (QUIC) atmospheric dispersion modelling system computes three-dimensional (3D) wind fields and plume transport and dispersion around buildings. It is designed to fill an important gap between extremely rapid but overly simplified flat-earth analytical models typically employed by the emergency response community and the high fidelity but computationally expensive computational fluid dynamics (CFD) codes (Brown et al. 2013). The QUIC system's empirical diagnostic wind solver, QUIC-URB, is based on the concept developed by Röckle (1990). The 3D mean wind field is initialized using one or more vertical profiles of wind speed and direction that can either be directly measured or an extrapolation from a single measurement point. The velocities are determined in horizontal planes between all of the profile locations using a two-dimensional Barnes-mapping interpolation scheme (Pardyjak et al. 2004). QUIC-URB then uses empirical parametrizations to modify the initial wind field to account for building effects (Brown et al. 2013) and vegetative canopy drag (Nelson et al. 2009). The QUIC system's urbanized Lagrangian random-walk atmospheric transport and dispersion model, QUIC-PLUME, employs standard planetary boundary-layer turbulence profile parametrizations (e.g., Rodean 1996) to estimate the vertical structure of the turbulence in nominally undisturbed flow and local gradient-based, non-local, and vortex mixing schemes in regions where building effects significantly modify the flow from the initial field (Williams et al. 2004).

The realism of atmospheric transport and dispersion modelling is highly dependent on the accuracy of the meteorological data that are used to drive the simulation. The principal meteorological quantities that affect atmospheric transport and dispersion within the atmospheric boundary layer are: wind direction, wind speed, atmospheric stability/turbulence parameters, and boundary-layer height (e.g., Pasquill and Smith 1984; Arya 1999). The 3D mean velocity field has the most significant effect since it determines the direction of travel, the speed at which the plume is advected downwind, and complex transport effects due to the vertical structure of the velocity field. The turbulence field has a secondary, but still significant effect, since it determines the lateral and vertical spread and subsequent dilution of the plume due to turbulent diffusion. This relationship between atmospheric conditions and the accuracy of the dispersion solution becomes even more complex when buildings and other obstacles influence the near-surface flow field. Brown et al. (2008) found that plume transport in cities can be very robust (i.e., unchanging) since the upper-level wind direction changes, and then suddenly shifts 180° at critical upper-level wind directions. Rodriguez et al. (2013) examined this issue in greater detail and demonstrated that the sensitivity of the dispersion pattern to the wind direction and source location is also influenced by patterns in the urban topography (eg. road/building network configurations, building sizes, size and orientations of urban canyons).

One of the principal challenges to performing accurate transport and dispersion modelling is obtaining all of the required meteorological information from established weather moni-

toring networks. Measurements of near-surface wind speed, wind direction, and temperature are common, particularly in populated areas where the release of airborne contaminants and the possible detrimental health effects are of greatest concern. However, standard weather stations rarely provide direct measurements of surface-layer turbulence and stability parameters such as the friction velocity (u_*), turbulent kinetic energy (e), surface heat flux, and Obukhov length (L), which are utilized by advanced atmospheric transport and dispersion models to determine the turbulent diffusion of airborne contaminants. The vertical structure in the atmospheric boundary layer, i.e., the wind direction, wind speed, temperature, and turbulence variation with height, is also important for contaminant transport and dispersion, but the spatial density of sodar, radar, and balloon-sounding networks is extremely sparse, and in the case of balloon-sounding measurements are typically only made at 12-h intervals. Furthermore, the boundary-layer height (h), which defines the vertical depth through which the plume can mix and is often used by atmospheric transport and dispersion models to account for vertical structure effects in the atmosphere, must often be approximated based on generalized diurnal cycle behaviour and may or may not account for local meteorological conditions at the time in question. The challenges associated with acquiring all of the meteorological information that affect the transport and dispersion of contaminants suggest that mesoscale numerical weather prediction (NWP) models, such as the Weather Research and Forecast (WRF) model (Skamarock et al. 2005) are attractive options for providing the input data required to drive microscale transport and dispersion simulations (Tewari et al. 2010; Chen et al. 2011; Wyszogrodzki et al. 2012).

Part 1 of this study (Nelson et al. 2016) investigated the WRF model's ability to replicate the wind velocity and turbulence observations from the Joint Urban 2003 field campaign (JU2003). Part 1 showed that significant differences were found between the observations and WRF model simulations of the meteorological parameters that are key to accurate atmospheric transport and dispersion modelling, namely: wind direction, wind speed, surface-layer turbulence, and boundary-layer height. The deviations in wind direction that were observed in Part 1 are consistent with previous investigations where the WRF model was coupled with microscale atmospheric transport and dispersion models (Tewari et al. 2010; Wyszogrodzki et al. 2012). The objective of assimilating mesoscale model fields into an urban dispersion model is to improve the accuracy of both the neighbourhood-scale and mesoscale transport and dispersion calculations, i.e., better prediction of the direction an airborne contaminant cloud travels after it is released, the geographic area covered by the plume, and the time history of the concentration field produced. The tracer-gas measurements from the JU2003 field experiment are used to evaluate the effects of the errors in predicted wind direction, resolved temporal scales, and the turbulence assimilation schemes on urban transport and dispersion model calculations. The primary goal of these analyses is to identify the challenges and potential sources of error that occur when driving an urban microscale atmospheric transport and dispersion model with a mesoscale reanalysis derived from a NWP model such as the WRF model. However, we also show that these same challenges affect transport and dispersion modelling in general regardless of whether a mesoscale model or on-site measurements are used to provide the necessary meteorological information.

2 Experimental Details

The JU2003 field campaign was performed from 29 June through 30 July 2003 and involved tracer-gas releases within the central business district of Oklahoma City, Oklahoma, USA
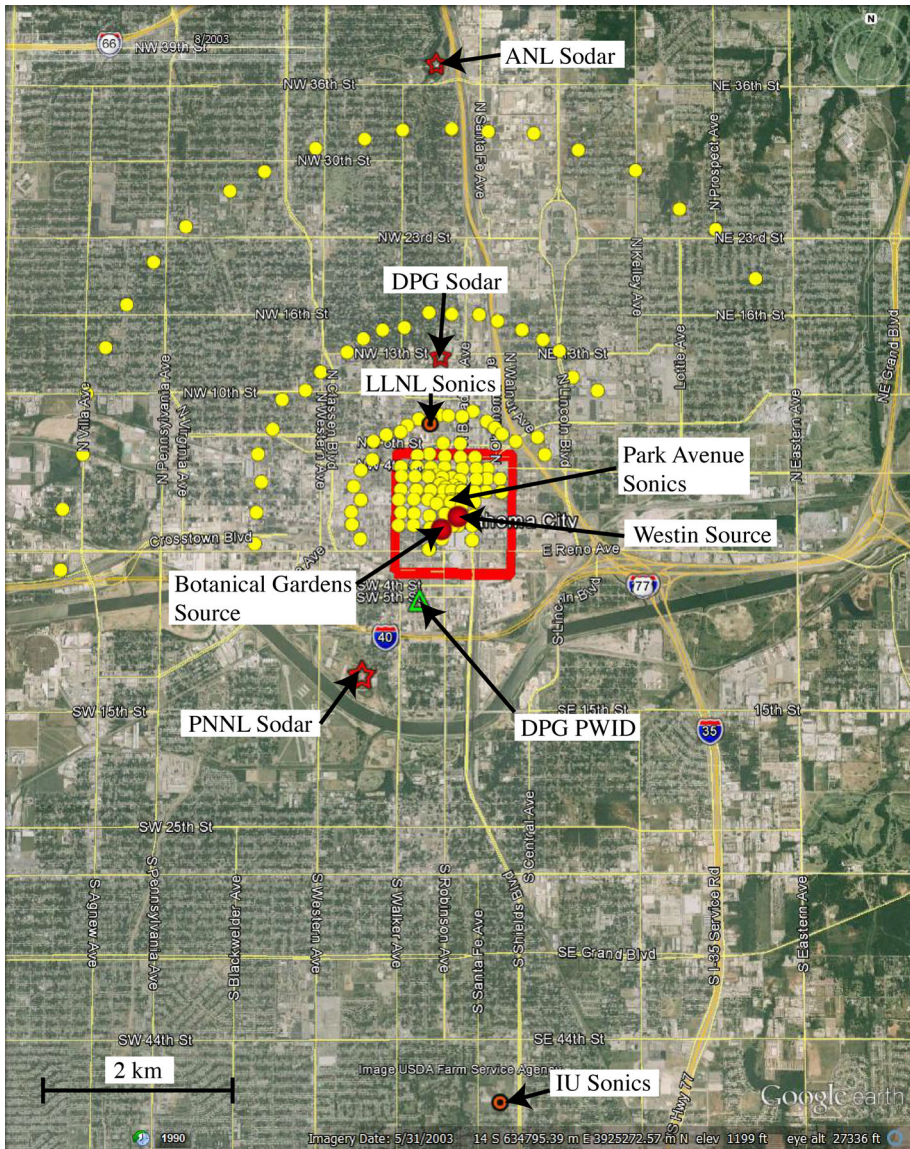
Fig. 1 Map of the locations of the wind sensors and tracer-gas samplers deployed in and around Oklahoma City during Joint Urban 2003 that are used in this work. Sampler sites are indicated by *yellow circles* and the source locations are denoted by *red circles*. The *red box* indicates the extent of the inner-grid simulation domain. Other important features are specifically labelled on the map. The satellite image is courtesy of Google Earth and the United States Department of Agriculture Farm Service Agency

(Allwine et al. 2004; Brown et al. 2004). Oklahoma City provided a relatively large urban area located in idealized terrain devoid of major natural topographical features. Figure 1 shows the locations of the tracer-gas samplers deployed in and around the urban core of Oklahoma City during JU2003. The samplers were deployed and operated by the National Oceanic and Atmospheric Administration's Air Resources Laboratory Field Research Division (ARL-FRD) and specific sampler details can be found in Clawson et al. (2005) and Allwine and

Table 1 Summary of the four releases studied in this manuscript

Case	IOP2-R1	IOP2-R3	IOP6-R2	IOP8-R2
Date	2 July 2003	2 July 3003	16 July 2003	25 July 2003
Release start (UTC)	1600	2000	1600	0600
Release start (CDT)	1100	1500	1100	0100
Release end (UTC)	1630	2030	1630	0630
Release end (CDT)	1130	1530	1130	0130
Release rate (kg s^{-1})	0.00501	0.00499	0.00318	0.00305
Total release (kg)	9.026	8.981	5.715	5.488
Release label	Westin	Westin	Botanical Gardens	Westin
Release UTMX (m)	634,773	634,773	634,603	634,773
Release UTMY (m)	3,925,887	3,925,887	3,925,763	3,925,887
Array orientation	South-east	South-east	South	South-east
Observed u_* (m s^{-1})	NA	0.68	0.62	0.73
WRF u_* (m s^{-1})	0.71	0.62	0.73	0.74
Observed $1/L$ (m^{-1})	NA	−0.0095	−0.011	0.0000026
WRF $1/L$ (m^{-1})	−0.0087	−0.014	−0.0091	−0.00083
Observed h (m)	1000	2000	780	340
WRF h (m)	1600	3500	1000	480

Array orientation indicates whether the 90° arcs of samplers were placed to ideally sample plumes under south-easterly or southerly wind directions. The 55-m sonic anemometer was used to measure the u_* and $1/L$ observations. Rawinsondes released from the PNNL sodar location at the beginning of the time period were used to derive the h observations

Flaherty (2006). Many of the samplers were clustered in the urban core (or central business district), which had an average building height of approximately 50 m (Burian et al. 2003). The tallest building in the urban core during JU2003 was approximately 152 m. While Fig. 1 shows all of the sampler locations deployed during the JU2003 campaign, not all of the locations were active during every tracer-gas release. The outer sampler arcs (nominally located at 0.5, 1, 2, and 4 km from the source locations) were restricted to a 90° sector that was rotated depending on the nominal wind direction that had been predicted the day before by NWP modelling (Liu et al. 2006).

There were ten, 8-h, intensive observation periods (IOPs) during JU2003 when atmospheric transport and dispersion experiments were performed. The first six IOPs were carried out during daytime and the final four IOPs were performed at night. Each IOP consisted of several instantaneous puff and 30-min continuous releases of SF$_6$ (see Clawson et al. 2005 for a full description of all the IOPs). This work utilizes data from four 2-h time periods: three daytime releases, IOP 2 Release 1 (IOP2-R1), IOP 2 Release 3 (IOP2-R3), and IOP 6 Release 2 (IOP6-R2); and one nighttime release, IOP 8 Release 2 (IOP8-R2). Specific details regarding the four periods used in this analysis including a comparison of the measured and simulated values of u_*, $1/L$, and h at the start of each release are found in Table 1. IOP2-R1 and IOP8-R2 have been used in several studies to evaluate atmospheric transport and dispersion model performance (Hanna et al. 2011; Brown et al. 2013; Kochanski et al. 2015). The four releases took place at two different release locations, which are referred to as Westin and Botanical Gardens, respectively, and shown as red circles in Fig. 1 (Clawson et al.

2005; Allwine and Flaherty 2006). Note that all Universal Transverse Mercator coordinates described here use Zone 14S of the World Geodetic System (WGS84) ellipsoid. Figure 1 also shows the locations of several instruments that are used to examine the mean wind and turbulence: the Pacific Northwest National Laboratory (PNNL) sodar; the Argon National Laboratory (ANL) sodar; the Dugway Proving Ground (DPG) sodar and portable weather information display (PWID) system, which is a sensor bundle that includes a prop-vane wind anemometer; and various sonic anemometers on the Indiana University (IU) tower upwind of the urban core, Lawrence Livermore National Laboratory (LLNL) downwind of the urban core, and Park Avenue street canyon within the urban core (see Allwine and Flaherty 2006; Nelson et al. 2007 for further information regarding the sonic anemometers located within Park Avenue).

The tracer-gas concentrations were measured using bag samplers that report the gas concentration in parts per trillion by volume. In order to convert parts per trillion by volume into kg m^{-3} the following relationship is used,

$$\chi = 10^{-12} C \frac{P M_w}{\Re T}, \tag{1}$$

where χ is the concentration in kg m^{-3}, C is the concentration in parts per trillion by volume, P is the atmospheric pressure in Pa, M_w is the molecular weight of tracer gas in kg mol^{-1} (0.146 kg mol^{-1} for SF$_6$), $\Re$ is the universal gas constant, and T is the temperature in K. We use dosage ($\mathscr{D}$), i.e., the time integrated concentration, in order to evaluate the total effect of the plume as it is transported downwind. A minimum dosage threshold of 5×10^{-7} kg s m^{-3} is used in the plots containing observations displayed herein to distinguish the plumes of the experiment from the background levels of SF$_6$, which were observed on the samplers throughout the experiment.

3 Simulation Parameters

The QUIC-system simulations used a nested domain with an inner grid depicted by the red box in Fig. 1. Buildings are explicitly resolved on the inner grid (see Fig. 2), which is surrounded by an outer grid where the buildings are not resolved. Table 2 lists the parameters that were common to all of the simulations presented here for both the inner and outer grids. The effects of individual buildings can be neglected once the plume grows sufficiently large relative to the size individual buildings. Nelson (2014) showed that including individual buildings outside of the inner-grid region of the simulations shown here had very little effect on the downwind plume simulations. While the QUIC system has the ability to approximate the effect of urban and/or vegetative canopies on the outer domain (Nelson et al. 2009), these have been omitted in order to isolate the effects of the turbulence import scheme on the downwind plume dispersion. The surface deposition and decay algorithms were disabled because the SF$_6$ tracer gas is inert.

The inner-most grid of the WRF model simulations used in these analyses had a nominal horizontal resolution of 3 km and cell-centres of the lowest four vertical grid cells of 20, 60, 120, and 180 m. As these dimensions are far larger than those used in either QUIC-system domain, the WRF model data had to be interpolated onto the domains of the QUIC-system simulations in order to provide smoothly varying wind and turbulence fields. The difference in the geographic projections used by the two models, the WRF model's use of latitude and longitude versus the QUIC system's use of Universal Transverse Mercator, makes the regular grid used by the WRF model in latitude and longitude behave as arbitrarily spaced data points

Table 2 Summary of the QUIC-system simulation parameters for both the inner and outer domains that are common for all of the simulations presented here

Simulation domain	Inner	Outer
South-west corner UTMX (m)	634,132	629,500
South-west corner UTMY (m)	3,925,308	3,924,000
East-west extent (m)	1180	10,000
North-south extent (m)	1210	8000
Vertical extent (m)	192	2000
Horizontal wind resolution (m)	5	50
Surface vertical wind resolution (m)	3	3
Maximum vertical wind resolution (m)	3	330
Horizontal dosage resolution (m)	5	5
Vertical dosage resolution (m)	3	3
Lagrangian timestep (s)	1	2
Release duration (s)	1800	–
Tracer particles	500,400	–

Note that no values are listed for the outer grid release duration and number of tracer particles because the particles initialized on the inner grid and are transferred to the outer grid as they leave the inner grid
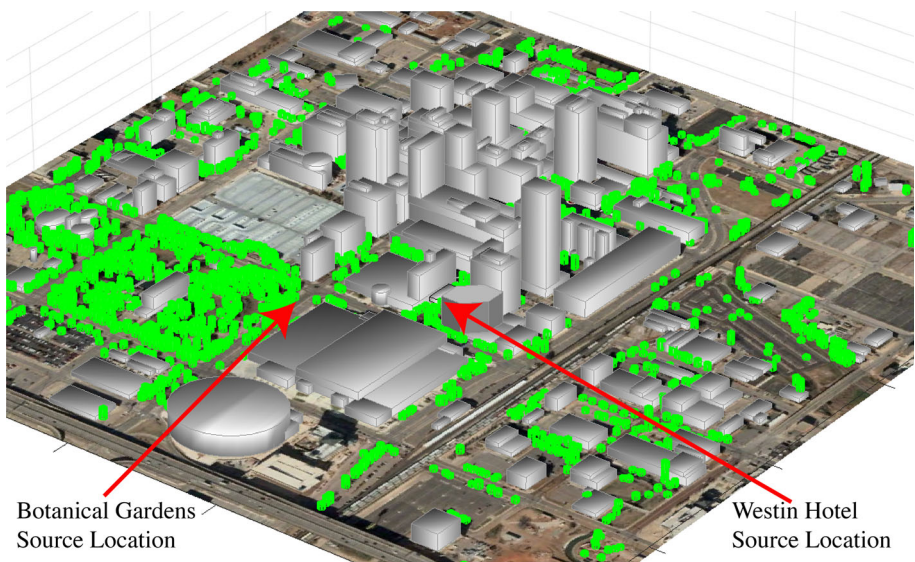

Botanical Gardens Source Location

Westin Hotel Source Location

Fig. 2 3D view of the inner domain used in the QUIC-system simulations as viewed from the south-east. The *bright green* elements are trees. The locations of the two source locations are indicated on the *diagram*. The satellite image is courtesy of Google Earth, the United States Department of Agriculture Farm Service Agency, and DigitalGlobe

within the domain of the QUIC-system simulations. QUIC-URB imports the velocity field using the horizontal position of the WRF model grid as a vertical profile of wind speed and direction that are interpolated using a quasi-3D Barnes objective map analysis scheme (Pardyjak et al. 2004). The QUIC system employs a k-nearest-neighbour search (Altman 1992; Bentley 1975) to significantly reduce the computational time needed to interpolate

large, arbitrarily-spaced datasets for all other WRF model data used by the QUIC system. Additionally the interpolation scheme linearly interpolates between the WRF model field time snapshots to the centres of the wind-field timesteps modelled by the QUIC system. By snapshots we refer to the fact that the data fields in the WRF model NetCDF output files simply consist of the current state of the field at that point in the simulation. However, the fact that the WRF model does not resolve microscale variations acts to average out all of the smaller-scale phenomena producing something similar to a running average.

There are several simulations presented here that do not use WRF model fields. A simulation was performed for each of the four scenarios that used the spatially varying observations from the PNNL sodar, ANL sodar, and the DPG sodar and PWID system (except for IOP2-R1 when the PWID system operation was sporadic), see Fig. 1 for sensor locations. All sodar measurements below 50 m were omitted due to surface effects and uncertainty at the bottom of the measurement range. Measurements from the top of the DPG and ANL sodar ranges were omitted conditionally based on their agreement with the measurements from the middle of the PNNL sodar range. As the spatial variability of the winds is likely to decrease with height above the surface, the PNNL sodar measurements above 250 m were used to supplement the upper-level wind observations at each of the other measurement sites. All profiles assume $z_0 = 0.6$ m to extrapolate wind measurements to the surface and use linear interpolation of $1/L$ and h observations (the first hour of these values are shown in Table 1) to calculate the turbulence fields associated with the resulting 15-min average mean wind fields. A $1/L$ value of -0.01 m^{-1} is assumed for IOP2-R1 due to the lack of observations from the IU tower during this time period. These simulations are intended to represent the best attempt by the QUIC system to simulate the observed plume dispersion using the available observations. Additionally the two cases from Brown et al. (2013), IOP2-R1 and IOP8-R2, assume neutral stability, use h values of 1,000 and 500 m, respectively, and use a single velocity profile for the entire 2-h simulation. Brown et al. (2013) used a roughness length (z_0) of 0.6 m and a wind speed at 5 m a.g.l. of 3.2 m s^{-1} ($u_* = 0.60$ m s^{-1}) for IOP2-R1 and z_0 of 1.0 m and 8.5 m s^{-1} wind speed at 80 m a.g.l. ($u_* = 0.78$ m s^{-1}) for IOP8-R2. The wind directions for the two cases were 215° (IOP2-R1) and 160° (IOP8-R2). Finally one simulation of the inner domain of IOP6-R2 uses 1-min averaged PWID system observations of wind speed and direction and a $z_0 = 0.6$ m to define the wind profile on the inner domain as well as the $1/L$ and h observations shown in Table 1 to account for the vertical structure in the turbulence of the simulation.

In order to avoid a lengthy description of the various wind and turbulence simulation parameters in the subsequent sections, we use the simulation labels as indicated in Table 3. An upper case P or I indicates the simulation uses WRF model fields. An upper-case P also indicates the WRF model turbulence was imported into the QUIC system simulations using parametrized profiles in the method described in Appendix 1.1. An upper-case I indicates that the turbulence was imported directly from the WRF model TKE (e) fields as described in Appendix 1.2. The labels for WRF-model-based simulations also indicate the length of the averaging period in min for wind direction correction (-15, -30, or -60). The wind direction was corrected using the 120-m level of the PNNL sodar. Simulations using uncorrected WRF model wind directions are labelled as—WRF; the simulations from Brown et al. (2013) are referred to as Brown. Simulations that use the spatially-varying winds as observed by the instruments shown in Fig. 1 are called OBS. A simplified CFD code called QUIC-CFD (Gowardhan et al. 2011; Neophytou et al. 2011) was used with 1-min averaged wind-velocity measurements from the PWID system to simulate the inner grid of IOP6-R2, and this simulation is called QCFD.

Table 3 Decription of the QUIC-system simulations

Simulation label	Inner domain data source	Outer domain data source	Update period (min)	Corrected direction	Turbulence scheme
P-WRF	WRF model	WRF model	15,15	No	Parametrized
I-WRF	WRF model	WRF model	15,15	No	Imported e
P-15	WRF model	WRF model	15,15	Yes	Parametrized
I-15	WRF model	WRF model	15,15	Yes	Imported e
P-30	WRF model	WRF model	30,30	Yes	Parametrized
I-30	WRF model	WRF model	30,30	Yes	Imported e
P-60	WRF model	WRF model	60,60	Yes	Parametrized
I-60	WRF model	WRF model	60,60	Yes	Imported e
Brown	Brown et al. (2013)	Brown et al. (2013)	120,120		Parametrized
OBS	PWID and sodars	PWID and sodars	15,15		Parametrized
QCFD	PWID	PWID and sodars	1,15		Parametrized

The meteorological data source for both the inner and outer simulation domains was one of the following: WRF model simulations, PWID system and/or sodar observations, or observations and the method described in Brown et al. (2013). The update period for the inner and outer simulation domains indicates how often the wind and turbulence fields were updated during the 120-min simulation. The next column indicates whether WRF model wind direction was corrected to match observations, where applicable. The turbulence scheme indicates whether the standard QUIC-system turbulence parametrizations (see Appendix 1.1) using either the spatially-varying WRF model fields or observations depending on the meteorological data source, or directly imported WRF model e (see Appendix 1.2) was used to produce ambient turbulence fields

4 Methods and Theory

4.1 The QUIC System Turbulence Parametrizations

The random-walk atmospheric transport and dispersion equations employed by QUIC-PLUME require the Reynolds shear and normal stresses as well as the TKE dissipation rate as inputs to generate the fluctuating velocities that simulate the effects of turbulence on the Lagrangian tracer particles (Williams et al. 2004). In order to avoid modifications to the WRF model, both of the QUIC system's WRF model turbulence-assimilation schemes have been based on standard fields available from WRF model simulations.[1] Specifically we use the u_*, h, $1/L$, and e fields. An examination of the literature reveals that all of the boundary-layer schemes that have been implemented in the WRF model have some biases in the surface-layer quantities that they predict (Lin et al. 2008; Hu et al. 2010; Xie et al. 2012). Even though the Mellor–Yamada–Janjic (MYJ) boundary-layer scheme uses local turbulence closure that may underestimate the vertical mixing under strongly unstable conditions (Hu et al. 2010; Xie et al. 2012), it was chosen due to its ability to directly export TKE fields. The QUIC system interpolates the relatively coarse WRF model fields onto the higher spatial resolution of the QUIC system's simulation domain. Two different methods of importing spatially varying surface-layer turbulence are explored: the first method uses the WRF model fields to provide the surface-layer parameters that are used in the QUIC system's turbulence model that is based on the parametrizations found in Rodean (1996). The second method uses the TKE fields of the WRF model directly. Specific details regarding how the two schemes

---

[1] A description of the NetCDF output files and the meteorological fields available therein can be found in Chapter 5 of the WRF model user's guide (Wang et al. 2015).

are used to produce the velocity variances needed by the random-walk dispersion model are found in the Appendix.

4.2 Performance Measures

Following Hanna and Chang (2012), quantitative indicators of the performance of the model using the predicted ($\mathscr{D}_p$) and observed ($\mathscr{D}_o$) airborne dosages are expressed by the fractional bias (*FB*), normalized mean-square error (*NMSE*), geometric mean (*MG*), geometric variance (*VG*), and percent of values within a factor of 2 and 5 (*FAC2* and *FAC5*). The indicators can be expressed as follows,

$$FB = \frac{2\overline{(\mathscr{D}_o - \mathscr{D}_p)}}{\overline{\mathscr{D}_o} + \overline{\mathscr{D}_p}}, \tag{2}$$

$$NMSE = \frac{\overline{(\mathscr{D}_o - \mathscr{D}_p)^2}}{\overline{\mathscr{D}_o} \times \overline{\mathscr{D}_p}}, \tag{3}$$

$$MG = \exp\left(\overline{\ln \mathscr{D}_o - \ln \mathscr{D}_p}\right), \tag{4}$$

$$VG = \exp\left(\overline{(\ln \mathscr{D}_o - \ln \mathscr{D}_p)^2}\right), \tag{5}$$

$$FACx = 100\frac{\left|\left\{\frac{1}{x} \leq \frac{\mathscr{D}_p}{\mathscr{D}_o} \leq x\right\}\right|}{\left|\left\{\mathscr{D}_p + \mathscr{D}_o > \mathscr{D}_t\right\}\right|}, \tag{6}$$

where $FACx$ is effectively the percentage of data points where either $\mathscr{D}_p$ or $\mathscr{D}_o$ is above a threshold dosage ($\mathscr{D}_t$) that are within a factor of x of each other. Note that the overbar indicates an averaged quantity; FB, $NMSE$, MG, and VG calculations do not include false positives, false negatives, or matched zero values; and the $FACx$ values include false positives and negatives but not matched zeros (Hanna and Chang 2012; Brown et al. 2013).

Warner et al. (2007) suggested using the measures of effectiveness (*MOE*), which compare the fraction of overlap between the predicted plume area (A_p) and the observed plume area (A_o) and the area of false positives (A_{fp}) and false negatives (A_{fn}), respectively. Since the plume is only observed at a discrete set of locations, the MOE are approximated by comparing whether $\mathscr{D}_o$ and/or $\mathscr{D}_p$ exceed $\mathscr{D}_t$. The number of sampler locations with: $\mathscr{D}_o$ above $\mathscr{D}_t$ (N_o), $\mathscr{D}_p$ above $\mathscr{D}_t$ (N_p), $\mathscr{D}_o$ above $\mathscr{D}_t$ but $\mathscr{D}_p$ below $\mathscr{D}_t$ (N_{fn}), and $\mathscr{D}_p$ above $\mathscr{D}_t$ but $\mathscr{D}_o$ below $\mathscr{D}_t$ (N_{fp}) are used as surrogates for A_o, A_p, A_{fn}, and A_{fp}, respectively. The MOE value converges to one for perfect overlap between the predicted and observed plumes,

$$MOE_{fp} = \left(A_p \cap A_o\right)\Big/A_o = \left(A_o - A_{fp}\right)\Big/A_o \approx 1 - N_{fp}\Big/N_o, \tag{7}$$

$$MOE_{fn} = \left(A_p \cap A_o\right)\Big/A_p = \left(A_o - A_{fn}\right)\Big/A_p \approx 1 - N_{fn}\Big/N_p. \tag{8}$$

The threshold-based normalized absolute difference (*NAD*) was proposed by Hanna and Chang (2012); it uses the overlap between the observed and predicted plumes, i.e., the number of sampler locations where both $\mathscr{D}_o$ and $\mathscr{D}_p$ are above $\mathscr{D}_t$ (N_{ov}). NAD values range between zero (perfect overlap) and 1 (no overlap),

$$NAD = \frac{0.5(N_{fp} + N_{fn})}{N_{ov} + 0.5(N_{fp} + N_{fn})}. \tag{9}$$

5 Analysis and Discussion

5.1 Wind-Direction Correction

Part 1 of this study found that the average absolute difference between the wind direction measured at the 120-m level of the PNNL sodar, and the direction from the WRF-model-simulated wind fields was 35° over the entire month of July 2003. In order to assess the performance of the two WRF-model-based turbulence schemes for the QUIC system, it is necessary to correct for the error in the predicted wind direction. Figure 3 shows the wind speed and wind direction predicted by the WRF model at a height of 120 m, compared with
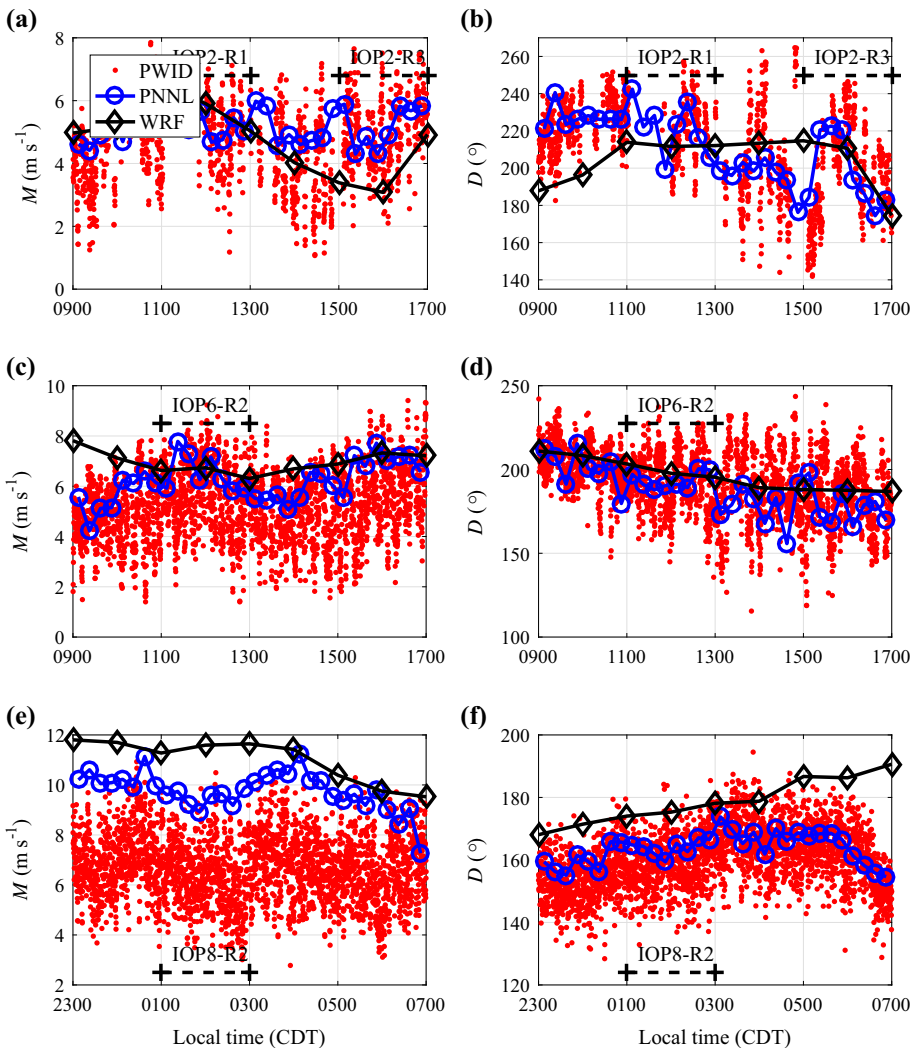

Fig. 3 Wind speed (M) and direction for IOPs 2, 6, and 8 as predicted by the WRF model (at 120 m) and measured by the PNNL sodar (at 120 m) and the DPG PWID system (i.e., prop-vane anemometer) above the Post Office building (at 40 m a.g.l.)

the wind speed and direction as measured by the 120-m level of the PNNL sodar. Also shown is the DPG PWID system, which was located at a height of 40 m. The first feature that is apparent in the comparison of the WRF model simulations and the observations is that the latter include intermediate-scale motions (small mesoscale or large microscale) that are not found in the WRF model simulations. The WRF model simulations vary smoothly from snapshot to snapshot at the top of each hour. Rather than instantaneous snapshots, the QUIC system expects ensemble-average wind and turbulence fields. However, since the WRF model simulations do not resolve these intermediate-scale fluctuations, the average conditions over a time period can be approximated by a linear interpolation between the WRF model field snapshots to the centre of the averaging period. This leads to the following question: what averaging period should be used to correct the wind direction predicted by the WRF model in order to enable the QUIC system to simulate the observed plume behaviour? We used 15-, 30-, and 60-min averages to explore the effect of temporal resolution of the wind field on the plume calculations. Simulations of IOP2-R1 and IOP2-R3 are more sensitive to the averaging period of the correction due to the high amount of variability in the observed wind direction during these releases. The wind direction is corrected by rotating all of the wind vectors throughout the 3D field by a constant offset in order to match the observed wind direction at the location of the observation.

The uncertainties in the measured mean wind direction by various instruments deployed around Oklahoma City made it difficult to choose a single wind direction for the analyses in Brown et al. (2013). The PNNL sodar measurements included lower levels that were closer to the height of the DPG PWID system, but these lower measurements exhibited much more variability. It is unclear whether this variability was due to local surface effects, or a result of limitations of the instrument in measuring the near-surface velocities. Eventually Brown et al. (2013) determined a single wind direction by performing several CFD simulations using a 20° arc defined by the variability in the observations. The prevailing direction was selected by comparing the simulated near-surface wind patterns with observations in the urban core (following Coirier et al. 2007). Here we wish to correct the ambient wind direction of the WRF model simulations, and therefore decided that it would be more appropriate to use the 120-m level of the sodar measurements.

The difference between the average wind speed measured by the PNNL sodar and the DPG PWID system is primarily due to the difference in the height of the measurements. Errors in the WRF model-predicted wind speed will also lead to errors in predicted plume concentrations since it is inversely proportional to wind speed (Arya 1999). We do not attempt to correct for errors in predicted wind speed as this is also related to the various turbulence quantities. It is unclear how to properly adjust all of the related turbulence properties in addition to the wind speed. As such, the wind speed is included as a reference for another source of error in the analyses that are presented here, particularly during IOP2-R3 and IOP8-R2.

5.2 Turbulence Parametrizations

Figure 4 compares the two methods of producing turbulence within the QUIC system from WRF model fields at the IU sonic tower for all four cases. This includes the measurements of TKE (e) by the sonic anemometers on the tower and the P-WRF, I-WRF, OBS, and Brown simulations (for IOP2-R1 and IOP8-R2). All other WRF-model-based simulations will have very similar TKE values depending on the turbulence import scheme. The TKE values resulting from parametrizations (see Appendix 1.1) using WRF model surface-layer parameters overestimates the observed TKE values. This overestimation of the observed
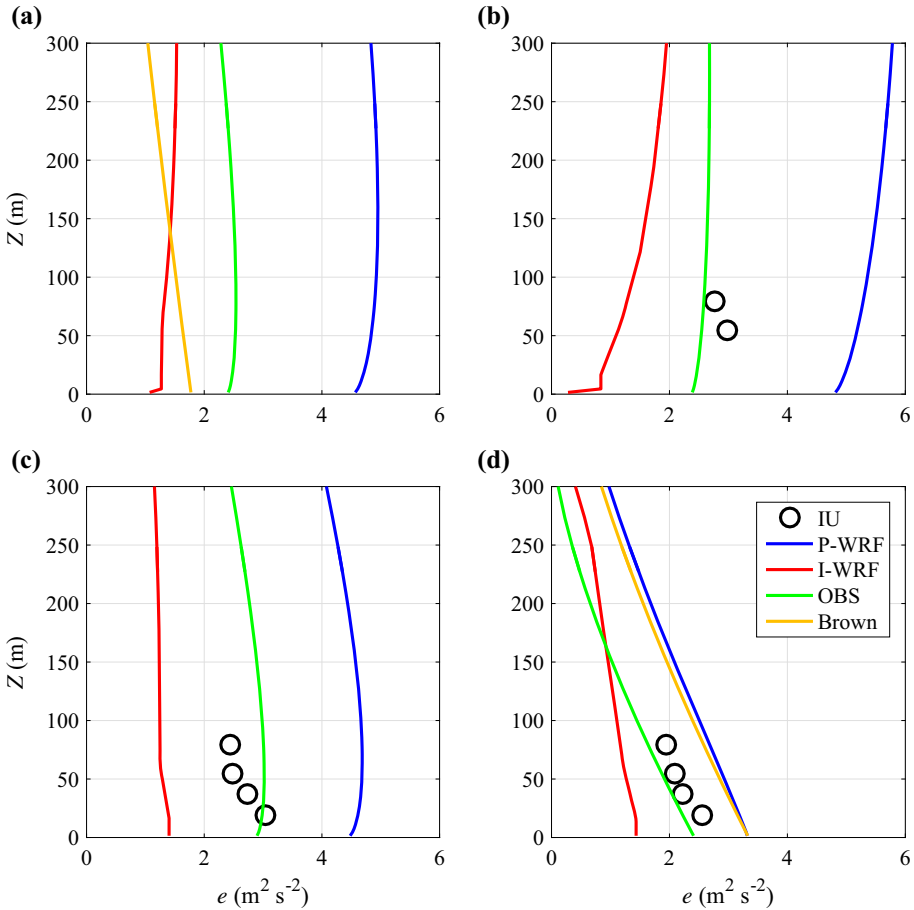
Fig. 4 Turbulent kinetic energy profiles at the IU tower during the first hour of **a** IOP2-R1, **b** IOP2-R3, **c** IOP6-R2, and **d** IOP8-R2

TKE values is principally due to the overestimation of h values (see Part 1 of this study and Table 1). The TKE fields that are imported directly from the WRF model (see Appendix 1.2) underestimate the observed TKE values. The QUIC system does not typically require u_* as part of the standard model inputs and instead calculates u_* for the turbulence profile parametrizations based on similarity theory and the near-surface velocity gradients. This is the method used to produce u_* values in the spatially-varying observations simulations and those from Brown et al. (2013). The IOP2-R1 simulation from Brown et al. (2013) produced turbulence similar to I-WRF, whereas the IOP8-R2 simulation is almost identical to the P-WRF turbulence profile. The OBS simulations, which are based on multiple spatially varying wind-field observations, provide the best approximation of the observed TKE in all three cases where observations were available. The assumed $1/L = -0.01$ m^{-1} during IOP2-R1 also produces a TKE profile very similar in magnitude to the observed TKE profiles from the other three cases and it is also between the two WRF-model-based turbulence schemes similar to the other three cases.

5.3 IOP 2 Release 1

Figure 5 shows the 165-, 275-, 500-, and 1000-m arcs of terrain-following near-surface airborne dosage from most of the simulations of IOP2-R1. By terrain following, we refer to the dosage profiles following the tops of buildings as well as changes in the surface elevation. All lateral dosage profiles presented in subsequent sections include the tops of buildings in the
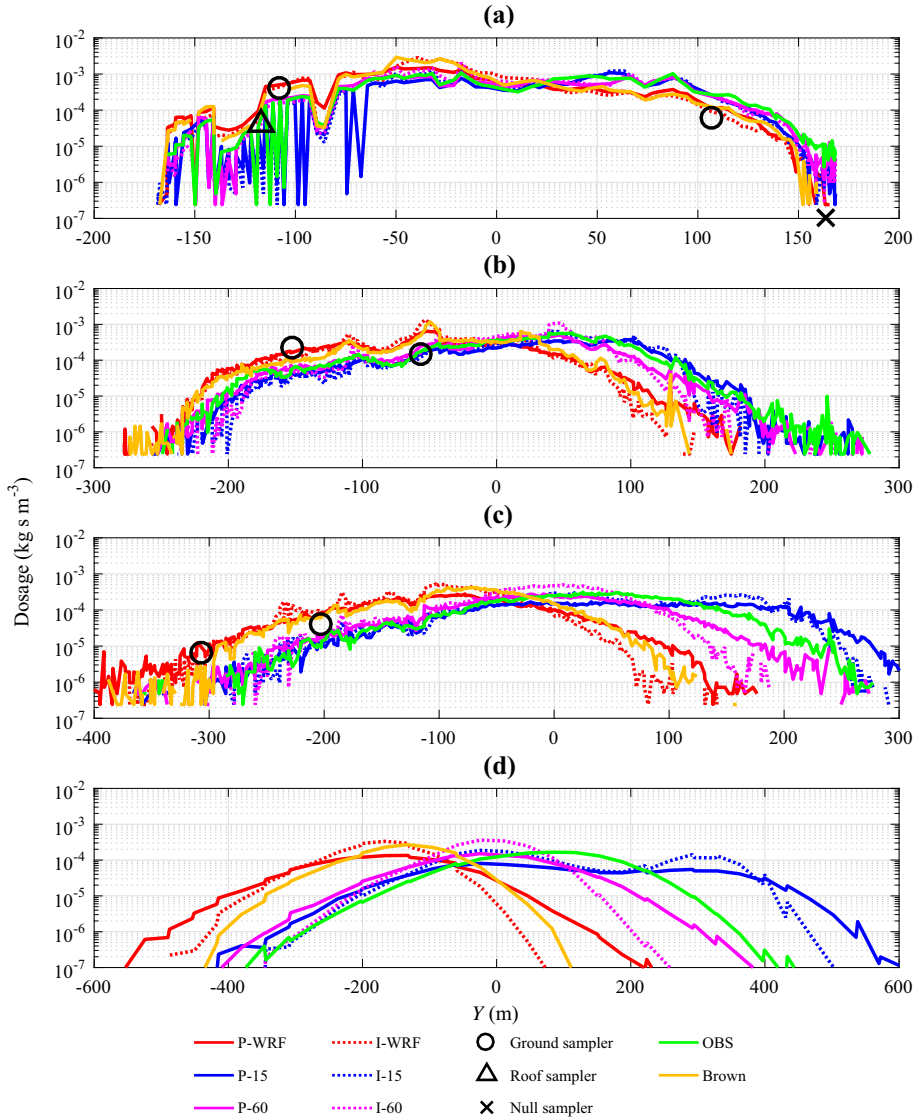

Fig. 5 Terrain-following airborne dosage collected during IOP2-R1 on 2 July 2003 from 1600 to 1800 UTC (1100 to 1300 CDT) along the 165-m (**a**), 275-m (**b**), 500-m (**c**), and 1,000-m (**d**) arcs compared with dosage simulated by the QUIC system. The source was placed at the Westin location shown in Fig. 1. Definitions of the simulation parameters are found in Sect. 3. Note that the lateral scale of the plots changes from arc to arc in order to show as much detail as possible on each arc

profile, whenever appropriate. It should be noted that the radial position of the observations in all dosage profile plots is nominal due to limitations in placing the individual samplers at specific radial position. All dosage profile arcs have been rotated into a coordinate system that is aligned with the initial plume trajectory (according to the 1-h average wind direction from the 120-m level of the PNNL sodar) and has an origin at the source location. This coordinate system makes X the downwind distance from the source and Y a measure of the lateral plume spread with positive and negative Y values indicating the eastern and western sides of the plume, respectively. Unfortunately, the prevailing wind direction caused the plume trajectory to miss most of the outer samplers for this release. The P-30 and I-30 simulations are omitted from Fig. 5 in order to improve readability of the plots as these simulations produce results between the 15-min and 60-min WRF model based simulations. Near the source, an overestimation of surface-level dosage on the eastern side of the plume can be seen in Fig. 5a. There is also little difference between any of the simulations. The effects of the underpredicted ambient turbulence imported directly from the WRF model cause the plume to be much more narrow than the overpredicted parametrized TKE plume. The effect of the turbulence scheme on the lateral spread is most evident on the 1-km arc. The I-60, I-WRF, and the Brown simulations all exhibit nearly identical lateral plume spread on all four arcs. This is in spite of the fact that all of the P-WRF and I-WRF simulations linearly interpolated wind speed and turbulence quantities from WRF model hourly snapshots every 15 min. This demonstrates the effect of the minimum resolved scales in the WRF model simulations, as the lateral plume spread of the corrected WRF-model-based simulations is dominated by the temporal resolution of the correction. Interestingly, neither the direction corrected WRF-model-based simulations nor the OBS simulation improve the simulated dosage profile on the 500-m arc, which was well simulated by the Brown, P-WRF, and I-WRF simulations. The corrected and OBS simulations would have predicted similar dosages if they had been rotated 50 m to the west along the 500-m arc, which equates to a 5° shift in wind direction. Therefore these differences could easily be explained by uncertainties in the wind direction measured by the sodars. Unfortunately, it is impossible to determine the effect that the spatial variability of the wind had on the plume transport further downwind, due to the plume missing the outer arcs. It would be reasonable to assume that the corrected WRF model-based simulations and OBS simulations are likely to perform better than the Brown, P-WRF, and I-WRF simulations with increasing distance from the source. The effect of spatially-varying wind fields is evident in the difference between the OBS simulation that used multiple sodars and the two WRF model-based simulations with 15-min averaged correction using only the PNNL sodar. The use of a single measurement under highly-variable wind fields, applies the intermediate scale variations in wind speed over the entire domain, effectively treating them as larger mesoscale variations. This produces enormous lateral plume spread, even in the case of I-15, which used the underestimated TKE fields from the WRF model. The use of multiple wind profiles limited the sphere of influence of the intermediate-scale variabilities in the OBS simulation, yielding a lateral plume spread similar to the P-WRF and P-60 simulations.

A summary of the statistical performance measures for all simulations of IOP2-R1 is found in Online Resource 1. Due to the fact that the prevailing wind direction carried the tracer gas off of the sampler grid, these statistics only include the near-source samplers. The P-WRF and I-WRF simulations had the best overall performance with a perfect overlap between the observed and predicted plumes. Additionally, 60 % of the predicted values are within a factor of two of the observed values and 100 % are within a factor of five. The Brown simulation has nearly as good performance to the P-WRF and I-WRF simulations. However as was noted above, a 5° difference in the predicted wind direction separated the simulations that performed well on the 500-m arc and those that did not, demonstrating the
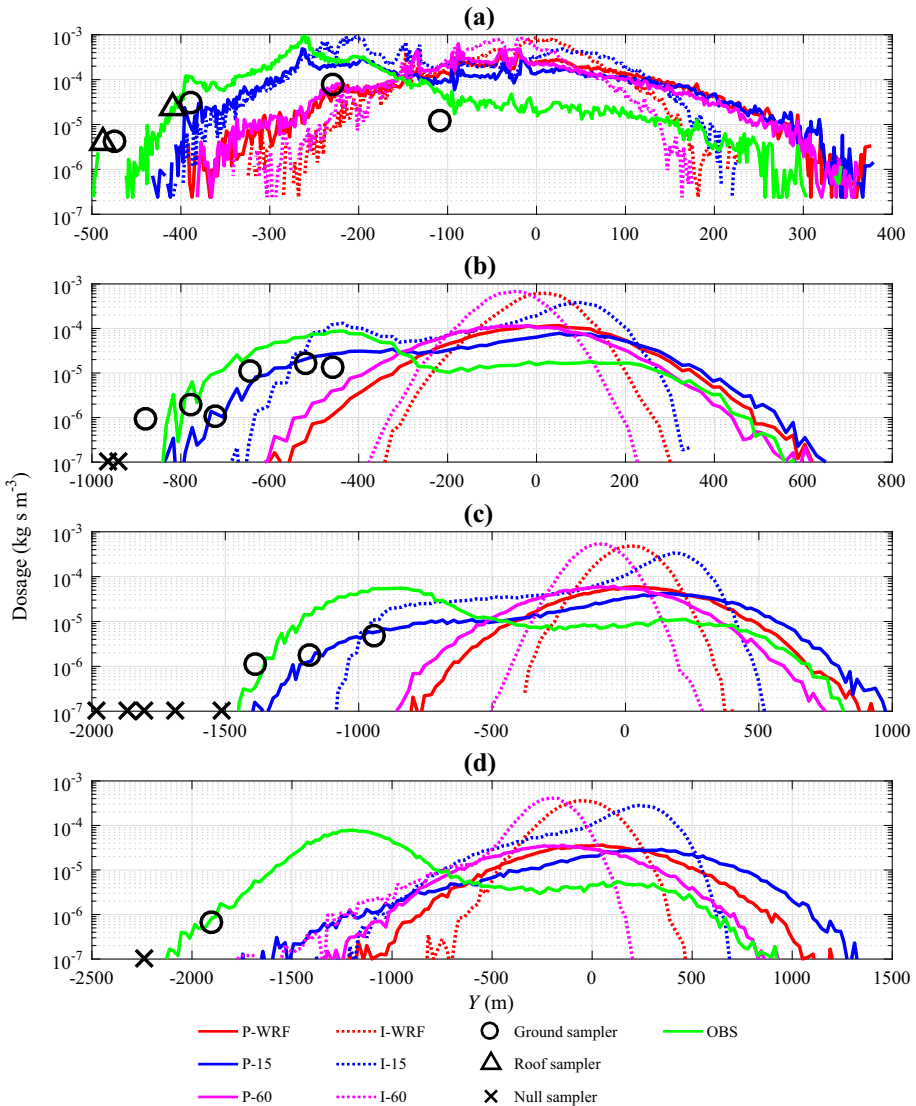
Fig. 6 Terrain-following airborne dosage collected during IOP2-R3 on 2 July 2003 from 2000 to 2200 UTC (1500 to 1700 CDT) along the 0.5-km (**a**), 1-km (**b**), 2-km (**c**), and 4-km (**d**) sampling arcs compared with dosage simulated by the QUIC system. The source was located at the Westin location shown in Fig. 1. Definitions of the simulation parameters are found in Sect. 3. Note that the lateral scale of the plots changes from arc to arc in order to show as much detail as possible on each arc

sensitivity of such analyses to small errors in wind direction. This sensitivity of the plume location accuracy to wind direction is consistent with the findings of Rodriguez et al. (2013).

5.4 IOP 2 Release 3

The effects of temporal resolution on the wind field can also be seen in the dosage arcs from IOP2-R3 in Fig. 6. Figure 3b shows that IOP2-R3 experienced even more wind variability

than IOP2-R1. The large shift in the prevailing wind direction in the latter half of IOP2-R3 occurred over large enough scales that the WRF simulations were able to simulate it. The P-15, I-15, and OBS simulations are the best at capturing the general plume behaviour observed by the samplers. The OBS simulation is the best at simulating the western edge of the plume and was the only simulation to match the positive collector on the 4-km arc. However, it overestimates the dosage values on the other arcs. P-15 provides better predictions of most of the dosages on the 1- and 2-km arcs, but does not produce enough lateral spread to accurately predict the westernmost positive samplers from the observations. This is in spite of the large overestimation of the observed turbulence seen in Fig. 4b. Larger averaging periods are unable to reproduce the observed lateral plume spread regardless of which turbulence scheme is used. While it is impossible to predict what might have been observed in the gaps between the sensors, the fact that the easternmost samplers on the 0.5-km arc encompass at least a local maximum in dosage along the arc suggests that there is a general tendency in the simulations to overpredict the peak dosages for this case. The underprediction of the wind speed seen in Fig. 3a could contribute to a consistent overprediction in the peak dosage for the WRF-model-based simulations. However, it does not explain the whole overprediction nor does it explain the overprediction by the OBS simulation. Figure 4b shows that the OBS simulation had the most accurate prediction of the ambient turbulence. The magnitude of wind-speed error in the WRF-model-based simulations would only account for a factor of two difference in the predicted dosages and the difference in the peak dosage is approximately a factor of 10. The predominant wind direction caused the plume to be only partially captured by the sampling array. Therefore, it is unclear whether the peak concentration was captured on any of the outer arcs. It is, however, evident that the PNNL sodar wind-direction measurement did not capture the full behaviour of the plume, particularly near the source. The fact that the winds were variable increases the likelihood of more spatial heterogeneity in the wind field, especially for shorter averaging times. The wind direction measured by the DPG PWID system in Fig. 3b shows additional rotation from the PNNL sodar measurement, which would push the plume farther west similar to the dosage observations. The failure of the OBS simulation to reproduce the western spread of the plume on the 0.5-km arc is likely due to these very small temporal variations that were not captured in the 15-min average. These small-scale variations could push the plume further west during part of the averaging period. The spatial heterogeneity during this release makes it inappropriate to correct the wind directions over the entire domain using the 15-min averaged winds from a single measurement location.

The performance measure summary for IOP2-R3 is shown in Online Resource 2. The performance measures confirm the superiority of the OBS simulation with the lowest number of false negatives and largest number of samples with both a factor of 2 and 5 percentages. The OBS simulation is closely followed by the P-15 simulation. Failure to properly account for the temporal and spatial variations in the wind field during this case had significant effects on the performance measures for all of the other simulations.

5.5 IOP 6 Release 2

Figure 7 shows the dosage arcs for IOP6-R2. Only the 15-min averaged wind direction correction is included in the plot, as the time resolution of the correction had little effect on the WRF-model-based plumes. Similar to the simulations of IOP2-R3, simulations of IOP6-R2 tend to overpredict the observed dosage values. IOP6-R2 provided the most ideal case for assessing the import of WRF model output during daytime conditions. In this case, the prevailing wind direction was aligned with the sampler arcs and was also nearly perpendicular to the predominant street-canyon direction. Additionally, the average wind direction remained
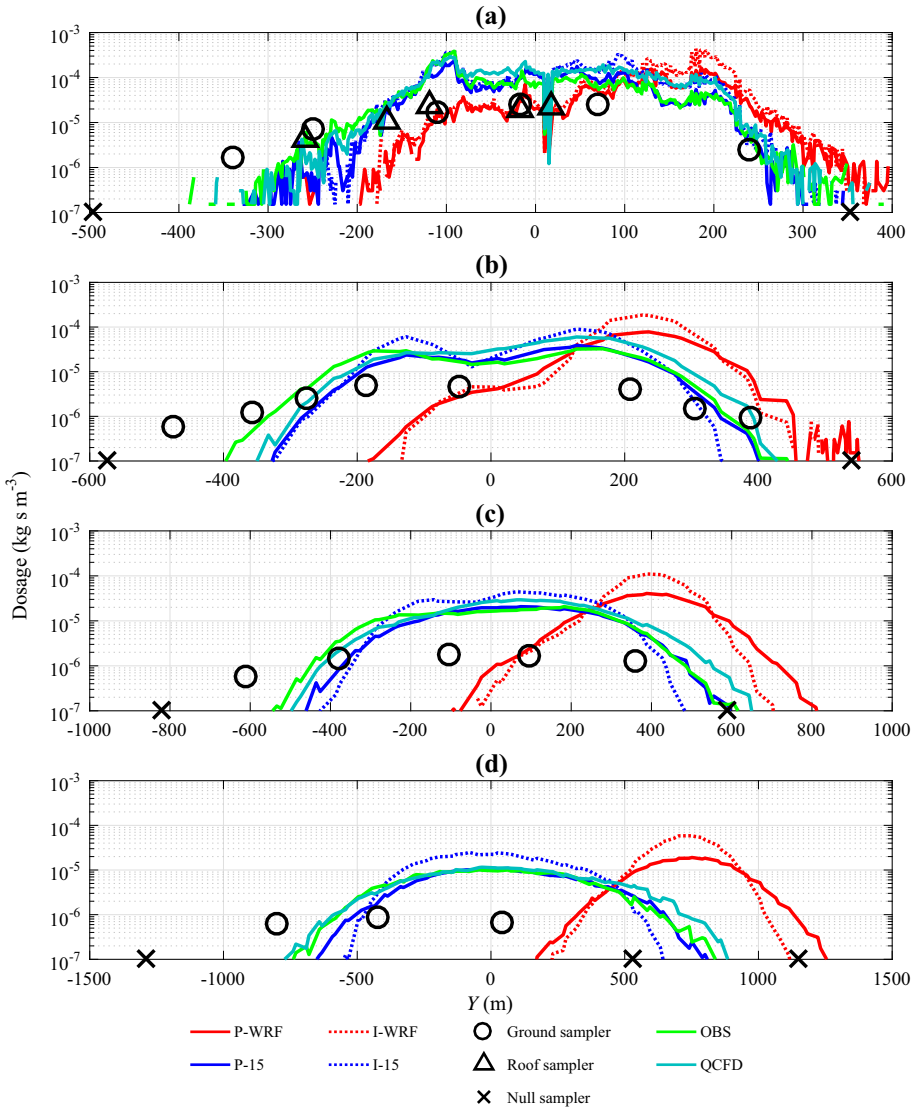
Fig. 7 Terrain-following airborne dosage collected during IOP6-R2 on 16 July 2003 from 1600 to 1800 UTC (1100 to 1300 CDT) along the 0.5-km (**a**), 1-km (**b**), 2-km (**c**), and 4-km (**d**) sampling arcs compared with dosage simulated by the QUIC system. The source was located at the Botanical Garden location shown in Fig. 1. Definitions of the simulation parameters are found in Sect. 3. Note that the lateral scale of the plots changes from arc to arc in order to show as much detail as possible on each arc

relatively steady throughout the 2-h period of the release (see Fig. 3d), and the wind speed was accurately simulated (see Fig. 3c). Even with these idealized conditions, none of the simulations accurately predicts the lateral spread of the plume. The QCFD simulation over-predicts the lateral spread on the eastern side of the plume. All simulations underestimate the lateral spread of the western side of the plume regardless of the time resolution of the wind-direction correction or the turbulence scheme used by the WRF-model-based simu-
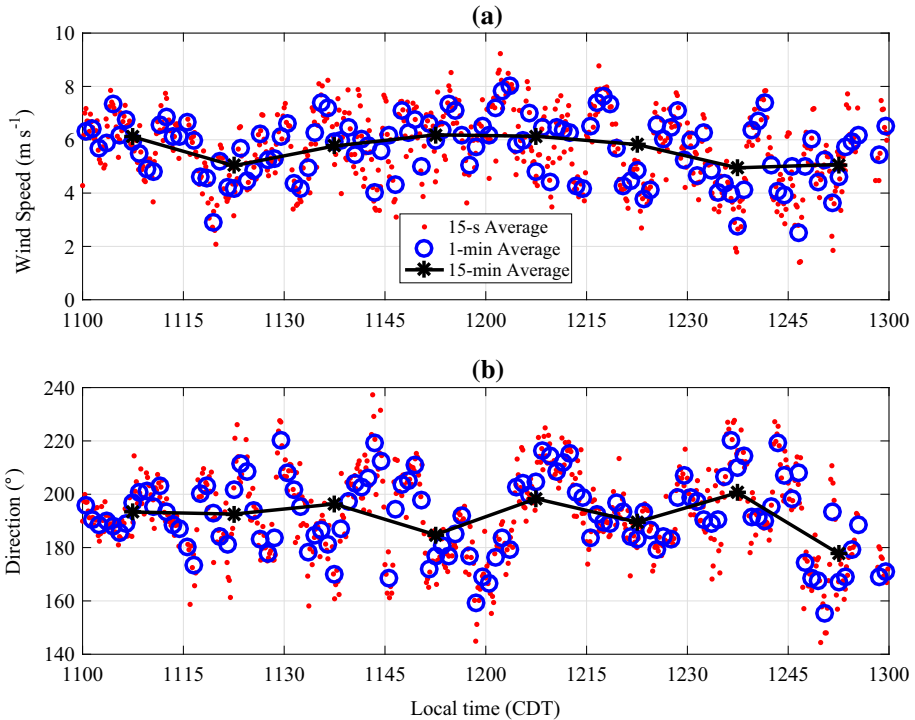
Fig. 8 Wind speed (**a**) and direction (**b**) as measured by the PWID system during IOP6-R2

lations. The OBS simulation, which accounted for the spatial variations in the wind field, was closest to reproducing the plume observations. Even the overpredicted turbulence of the parametrized WRF model turbulence scheme (see Fig. 4c) underpredicted the lateral spread on the western edge of the plume. A closer examination of the DPG PWID system data (see Fig. 8) indicates that the steady 15-min average wind direction is actually due to oscillating over smaller time scales. The wind direction had a 15-min period during the first 15 min of the release and 7-min period during the last 15 min of the release. The flow oscillates between 160° and 230° in the raw 15-s average data, and 175° and 220° in the 1-min averaged data. Outside of the urban core, one would naturally consider these motions as large-scale turbulence, however it is less obvious how these types of oscillations should be treated within the urban core.

The maximum dosage observed by any of the samplers during IOP6-R2 was significantly lower than any of the other cases examined here, even when normalizing by the different release amounts for each of the cases. One would expect sudden large-scale shifts in wind direction, such as those that were observed during IOP2, would produce lower dosages. A sudden shift in wind direction would cause the elongated plume to act as a line source that is then transported with the new wind direction. One would also expect the enhanced mixing that occurs under highly convective conditions to produce lower dosages as the plume mixes vertically with the thermal cells. While the above-mentioned phenomena can certainly yield lower concentrations and dosages, they do not appear to play a significant role in the relatively low dosages observed during IOP6-R2. The 15-, 30-, and 60-min averaged wind fields were very steady over the period with the release, therefore sudden shifts in the large-scale wind

direction were not a factor. IOP2-R3 was conducted under much more convective conditions as evidenced by the much larger value of h that was observed during IOP2-R3, see Table 1. The fact that the ambient TKE value was accurately reproduced by the OBS simulation, which also used observed wind profiles and still overpredicted the observed near-surface dosages suggests that this is associated with another factor.

The combination of the near-southerly prevailing wind direction (nominally perpendicular to the long dimension of rectangular blocks of buildings in Oklahoma City's urban core) and the small-scale oscillations in the wind direction likely caused the channelling to switch between redirecting the near-surface flow to the east and west. This oscillation in the near-surface flow would naturally lead to enhanced lateral spread of the plume and therefore lower peak dosages. Figure 9 shows the near-surface dosages from the inner-grid from, (a) the OBS simulation using the 15-min averaged spatially-varying observations, and (b) the QCFD simulation using 1-min averaged wind observations from the PWID system. Note the large lateral spread in the observations that extend nearly perpendicular to the predominant wind direction. This is most evident in the samplers immediately to the north-west and to the east of the source location, both of which are significantly underpredicted in the OBS simulation. The QCFD simulation, which uses 1-min PWID system data, does improve the western extent of the observed plume, nearly matching the ≈ 0.0001 kg s m^{-3} observation to the north-west of the source location. However, it is still unable to reproduce all of the low-level plume observations on the western edge of the inner domain. There is a large underground parking structure to the north of the Botanical Gardens, and this parking garage could explain the positive sampler near the south-west corner of the parking garage. It may be trapping and transporting a portion of the plume to the western side of the parking garage. The inability to reproduce the lateral transport on the western side of the plume is in spite of the fact that the 1-min averaging time makes double counting the contribution of the oscillations in wind direction through the time-varying mean and turbulence fields likely. The QCFD simulation overestimates the lateral plume spread on the eastern edge of the plume. This overestimation of the effects of channelling on the eastern edge of the plume might be due to the fact that individual wind timesteps in the QUIC system are generated as if the wind field is in steady state. At 1-min time scales, the winds will certainly not be in a steady state throughout the urban core. The flow that channels down the long street canyons may run into the flow that begins to enter the other end of the street canyon, as the prevailing wind direction shifts. Such an interaction could produce large updraughts, as there would temporarily be a convergence zone, where the two masses of air run into each other. Similarly, a large downdraught on the other end of the canyon would be produced, where the prevailing flow is suddenly no longer into that end of the canyon, resulting in a divergence zone. If these types of motions occur close to the source, it would significantly affect the surface-level dosages. The effect of the trees is seen in the positive sampler to the south of the source location. QUIC-CFD does not currently account for the effects of vegetation canopies. All of the simulations that include vegetation transport the plume south, which was also found in the observed plume. It is noteworthy that these near-source effects propagate downstream and are evident in the 4-km arc (Fig. 7d). It is also interesting that such complex behaviour should be found in a scenario that would normally be considered highly idealized. The mean wind direction that is both steady and nearly perpendicular to the street canyons make this case similar to the conditions employed in countless numerical and laboratory wind-tunnel studies. This clearly demonstrates the complexity in predicting urban-plume dispersion under real-world conditions.

The summary of the performance measures for all simulations of IOP6-R2 are found in Online Resource 3. It is interesting to note that while the OBS simulation provided the best
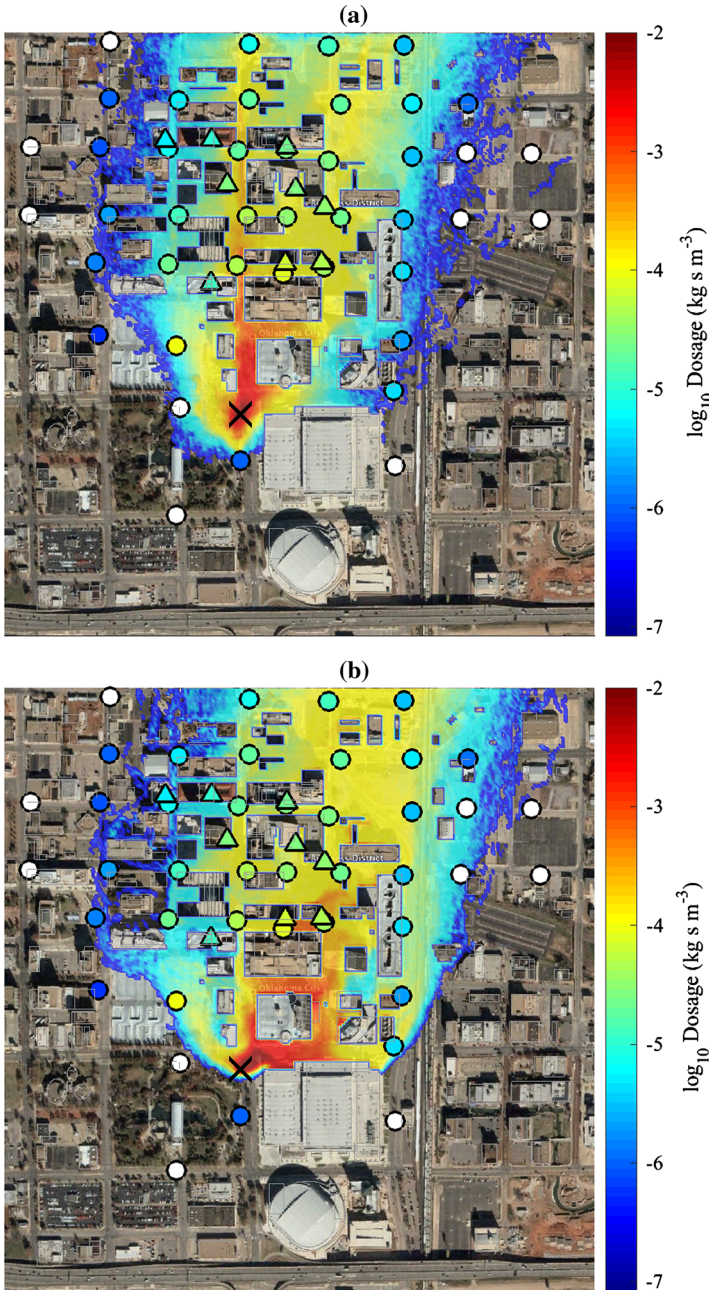
(a)

(b)

Fig. 9 Near-surface airborne dosage from IOP6-R2 using the OBS simulation with 15-min averaged winds (**a**) and the QCFD simulation that uses 1-min PWID system wind speed and direction input and standard turbulence algorithms in the QUIC system (**b**). The source was located at the Botanical Garden location shown in Fig. 1. *Circular symbols* indicate near-surface observations and triangles indicate rooftop observations. The source location is indicated by the *black X*. Trees are not shown in order to avoid confusion with the plume contours. The satellite image is courtesy of Google Earth, the United States Department of Agriculture Farm Service Agency, and DigitalGlobe

prediction of the plume spread in the total number of overlapping samples and matching observations within a factor of five, the I-WRF and P-WRF simulations actually provided significantly more observations within a factor of two. This is in spite of the fact that they obviously did not perform as well on the outer arcs as shown in Fig. 7. The 0.5-km dosage arcs in Fig. 7a shows that the improved number of predictions within a factor of two of the observations is actually due to wind direction error. The wind direction error causes the off-centreline predictions to be compared with the peak dosage observations. This demonstrates the danger in relying on only a few performance measures to evaluate the performance of a model, since these can at times be deceptive.

5.6 IOP 8 Release 2

The terrain-following arc dosage profiles from IOP8-R2 are shown in Fig. 10. As was the case with IOP6-R2, there is little dependence on the time resolution between the 15-, 30-, and 60-min averaged periods for the wind-direction correction. Therefore, only the 15-min averaged corrections are included in the figure. The correction using the PNNL sodar certainly improves the plume simulations. However, the method described in Sec. 5.3, which was employed by Brown et al. (2013) to select the predominant wind direction, provides a superior simulation of the observed plume travel on the outer arcs. This is in spite of the fact that a uniform velocity profile was used for the entire duration of the simulation. The OBS simulation also performs very well, but both the Brown and OBS simulations underpredict the observed dosage along the western edge of the 0.5- and 1-km arcs. In fact, there is only a $\approx 3°$ difference in the trajectory between the two simulations that best reproduced the observed plume and the corrected WRF-model-based simulations. Similar to the simulations of the other cases, higher dosages are found in the predicted arcs than are found in the observations. However, in this case, the peaks in the 0.5-km arc occur in the gaps between the samplers and the Brown and OBS simulations provide good estimates of the dosages at the sampler locations. It is possible that higher dosages on the 0.5-km arc could have been observed had more samplers been available, but this can obviously not be verified. The 1- and 2-km arcs indicate that the simulations are starting to overpredict the observed dosage, similar to the simulations of the daytime cases. The lateral plume spread is slightly underpredicted by the Brown and OBS simulations along the 2-km arc even though the OBS simulation had the best match to observed ambient turbulence quantities and the Brown simulation overpredicted them (see Fig. 4d). The near-source building effects are also evident on the 0.5 km arc profile in Fig. 10a. The dosage arcs do not exhibit particularly Gaussian behaviour nearest the source, as they are skewed to the eastern side of the plume. However, the plume smooths out with downwind distance and transitions to more Gaussian-like behaviour on the outer arcs.

Not only does the time resolution have very little effect on the downwind profiles for this case, but neither does the turbulence scheme for the WRF-model-based simulations. This is surprising due to the difference in the ambient turbulence produced by the two schemes as seen in Fig. 4d, where the parametrized turbulence scheme produced approximately twice the values of the turbulence directly imported from the WRF model TKE fields. Figure 11 shows the dosage profile arcs of the P-60 and I-60 simulations of IOP8-R2 that both include and exclude the building effects on the inner grid. Excluding the building effects on the inner grid makes the effects of the ambient turbulence easily distinguishable. Thus the lack of significant differences between the two turbulence import schemes in Fig. 10 is due to the fact that the building effects on the inner grid dominate the lateral spread over the first few km downwind of the source. The amount of ambient turbulence eventually produces differences in lateral spread on the 4-km arc (see Fig. 11d).
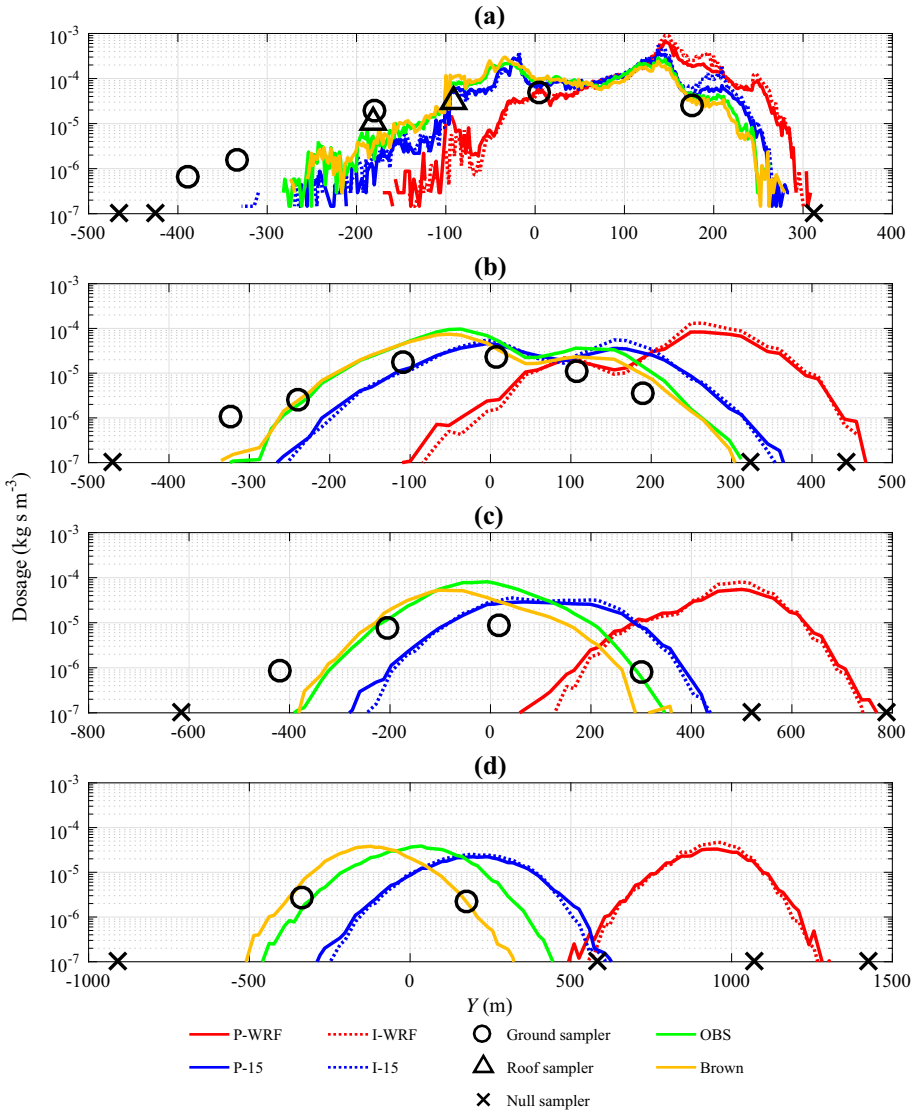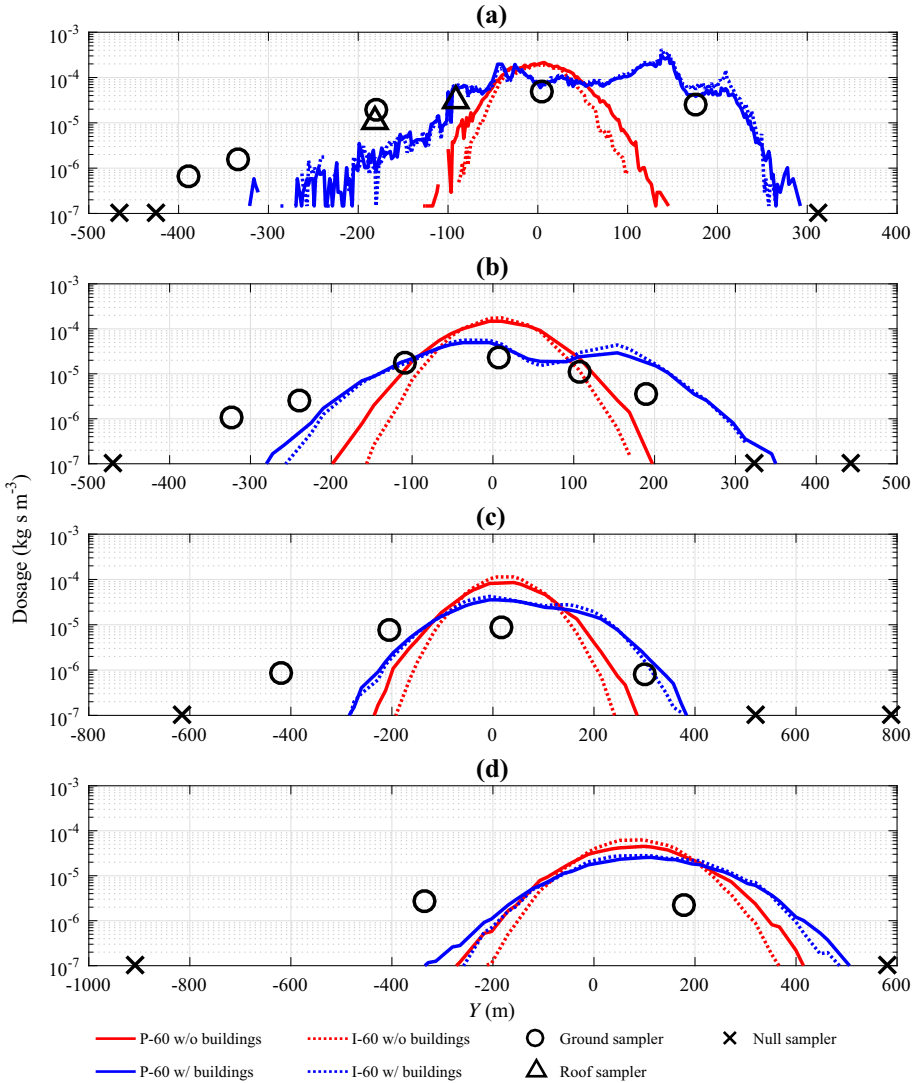
Fig. 10 Terrain-following airborne dosage collected during IOP8-R2 on 25 July 2003 from 0600 to 0800 UTC (0100 to 0300 CDT) along the 0.5-km (**a**), 1-km (**b**), 2-km (**c**), and 4-km (**d**) sampling arcs compared with dosage simulated by the QUIC system. The source was located at the Westin location shown in Fig. 1. Definitions of the simulation parameters are found in Sect. 3. Note that the lateral scale of the plots changes from arc to arc in order to show as much detail as possible on each arc

The summary of the performance measures for IOP8-R2 are listed in Online Resource 4. As one would expect given the surface-level dosage profiles shown in Fig. 10, the Brown and OBS simulations of IOP8-R2 have the best performance statistics of any of the cases, particularly regarding the $FAC2$ score. As was mentioned above, there was only a 3° difference in trajectory between the best two simulations and the corrected WRF-model-based simulations. This small error in wind direction resulted in halving the $FAC2$ score. While

Fig. 11 Terrain-following airborne dosage collected during IOP8-R2 on 25 July 2003 from 0600 to 0800 UTC (0100 to 0300 CDT) along the 0.5-km (**a**), 1-km (**b**), 2-km (**c**), and 4-km (**d**) sampling arcs compared with dosage simulated by the QUIC system. The source was located at the Westin location shown in Fig. 1. All cases have a corrected wind direction using 60-min averaging period and use either parametrized turbulence from surface-layer similarity parameters exported from the WRF model or turbulence imported directly from WRF, model output and either include or exclude inner-grid building effects. Note that the lateral scale of the plots changes from arc to arc in order to show as much detail as possible on each arc

wind-direction correction improves the performance of all of the WRF-model-based simulations, it is interesting to note that the 60-min averaging period significantly improves the performance over the 15- and 30-min averaging periods. This is due to the longer time period averaging out small errors in the observed wind direction from the PNNL sodar.

6 Conclusions

The QUIC system has been modified in order to ingest meteorological fields from WRF model simulations. The WRF model fields are used to initialize both the QUIC system's mean wind fields and several other meteorological quantities that affect atmospheric transport and dispersion. While there was one case where the uncorrected WRF model wind direction produced plume simulations that outperformed the simulation that used on-site observations from multiple sodars, the 35° mean absolute difference between the WRF-model-predicted and observed wind direction over the entire month of July 2003 (see Part 1 of this study) suggests that this instance of the WRF model outperforming on-site observations was serendipitous. In fact the difference in wind direction in this instance was only 5°, which could easily be due to errors in the measured wind direction. The use of spatially-varying observations outperformed all of the WRF-model-based simulations for the other three cases that were examined here. The method employed by Brown et al. (2013) was able to further improve the predominant wind-direction estimate for the two cases that they examined by matching near-surface wind patterns within the urban core produced by CFD simulations to observed patterns. While the method employed by Brown et al. (2013) produced the best results for the small sample of cases presented here, it is highly time and labour intensive and is therefore completely impractical for use in most instances. Additionally, the density and quality of observations used to produce the observation-based simulations, was far more than would ever be found in any standard meteorological sensor network, and yet it was still difficult to match the basic plume trajectory for some of the cases analyzed here. These demonstrate the challenge of determining an accurate measure of what is arguably the most fundamental and important quantity affecting the accuracy of atmospheric transport and dispersion modelling. Further research is required in developing a simple and systematic method for accurately determining the prevailing wind direction over the neighbourhood scale.

Two methods have been developed to calculate the turbulence quantities required by QUIC-PLUME's Lagrangian random-walk dispersion model from the WRF model fields. The first method uses the WRF model u_*, $1/L$, and h fields in empirical parametrizations of the turbulence within the planetary boundary layer. The second method directly imports the WRF model's 3D TKE field, if it is provided by the boundary-layer scheme used in the WRF model simulations, such as the MYJ scheme used here. The 3D TKE fields from the MYJ boundary-layer scheme underpredicted the observed TKE values, which was found during both thermally stable and unstable conditions in Part 1 of this study. The WRF model turbulence import scheme using empirical parametrizations consistently overpredicted the observed TKE values. The standard turbulence model in QUIC-PLUME using observed h values, $1/L$ values, and wind fields was able to replicate the observed turbulence very well. Since the first method for importing turbulence from the WRF model uses the same empirical parametrizations as the standard QUIC-PLUME turbulence model, the overprediction of turbulence in the WRF model-based simulations was due to errors in the WRF model field. The over prediction of h by the MYJ boundary-layer scheme was the primary cause of the overprediction of turbulence. The performance of other WRF model boundary-layer schemes will be evaluated in the future.

The WRF model mean wind fields were not able to reproduce the intermediate scale (i.e., between mesoscale and microscale) temporal and spatial variability that was found in the observations. The large temporal and spatial variability that occurred during IOP2 caused the corrected WRF-model-based simulations to significantly overpredict the lateral spread of the plume because the wind-direction corrections only used a single measurement location.

Thus local intermediate-scale variabilities were treated as if they were sudden changes in the mesoscale wind field. Even in cases that had relatively steady mean wind direction throughout the release, such as IOP6-R2 and IOP8-R2, the effects of subtle variations in the mean wind field increase with downwind distance. In fact a difference of only 3° in the predicted plume trajectory during IOP8-R2 caused the simulation following Brown et al. (2013) and the simulation using spatially-varying observations to have $FAC2$ scores that are twice the values of the WRF-model-based simulations that were corrected with a single measurement location.

The analyses presented here also demonstrate the significant effects of buildings on the near-source atmospheric transport and dispersion of contaminants in the urban environment. These building effects were shown to dominate the plume spread of IOP8-R2, where little difference was seen between the two WRF model turbulence import schemes in spite of a factor of two difference in the predicted turbulence levels. IOP6-R2 had very steady 15-, 30-, and 60-min averaged wind directions that were nearly perpendicular to the predominant street-canyon direction, but oscillations were observed in the wind direction with a period ranging between 7 and 15 min over the release. This likely contributed to the rapid near-source plume spread and lower peak dosages that none of the simulations were able to replicate, even when using the 1-min averaged winds measured by the PWID system and the higher-fidelity QUIC-CFD wind simulations. While these oscillations would normally be treated as large-scale variability in undisturbed surface-layer flow, the scales imposed on the flow by the buildings within the urban core make treating these oscillations as large-scale turbulence inappropriate within the urban canopy. It is possible that oscillations in the prevailing wind direction may be cause complex interactions as the flow oscillates back and forth in the street canyons. It would be instructive to investigate whether or not a large-eddy simulation, such as Lundquist et al. (2012), would be able to accurately predict the observed behaviour of this release. Large-eddy simulation has the potential of reproducing the complex transient flow interactions that the oscillations in the prevailing wind direction could produce within the street canyons and therefore might be able to simulate the low near-surface dosage levels. Other complex phenomena such as infiltration into and subsequent exfiltration out of the underground parking garage just north of the Botanical Gardens due to the ventilation systems that are typically used in these structures may also be a factor in producing the observed lateral plume spread. Both possible explanations for the overprediction of simulated near-surface dosages should be further investigated in the future.

Appendix

Appendix 1.1: Turbulence Derived from WRF Model Surface-Layer Parameters

Due to the diagnostic nature of the QUIC-URB wind solver, only 3D mean wind fields are produced without turbulence quantities. In the absence of further information regarding the turbulence structure in the planetary boundary layer, which is required by the Lagrangian random-walk dispersion model, the turbulence must either be inferred from the mean wind

field or parametrized using surface-layer parameters such as u_*, $1/L$, and h. By default, the QUIC system uses a combination of parametrized turbulence profiles (in regions that are nominally undisturbed by explicitly resolved building effects), local gradient (in regions near where building flow parametrizations have been applied), and enhanced non-local turbulence schemes (in some building-flow parametrization regions). Williams et al. (2004) has a complete description of the methods employed by the QUIC system to deduce turbulence in and near the building flow parametrizations. The WRF model fields of u_*, $1/L$, and h that have been interpolated onto the domain grid of the QUIC system simulation are used as local values within the parametrizations used by the QUIC system's standard turbulence scheme to yield the 3D spatially-varying turbulence fields required by the Lagrangian random walk dispersion model.

In the surface layer, dimensional analysis combined with empirical observations have confirmed Monin-Obukhov similarity theory, which provides standard relationships between u_*, L, and the mean wind speed (Monin and Obukhov 1954; Calder 1966; Stull 1988; Arya 2001). The QUIC system uses parametrizations of the variation of turbulence with vertical position based on surface-layer quantities and h as described in Rodean (1996). For neutral to stable thermal stabilities ($z/L \geq 0$), the QUIC system uses the following relations for the velocity variances (σ^2) in a local coordinate system rotated such that the u-velocity component is in the local mean wind direction,

$$\sigma_u^2 = u_*^2 \left(6.3 \left(1 - \frac{z}{h} \right)^{3/2} \right), \tag{10}$$

$$\sigma_v^2 = u_*^2 \left(4.0 \left(1 - \frac{z}{h} \right)^{3/2} \right), \tag{11}$$

$$\sigma_w^2 = u_*^2 \left(1.7 \left(1 - \frac{z}{h} \right)^{3/2} \right). \tag{12}$$

For thermally unstable conditions ($z/L < 0$), another thermal-stability dependent term is added to Eqs. 10–12, which accounts for the generation of turbulence due to buoyancy under thermally unstable conditions, yielding the following relations,

$$\sigma_u^2 = u_*^2 \left(6.3 \left(1 - \frac{z}{h} \right)^{3/2} + 0.6 \left(-\frac{h}{L} \right)^{2/3} \right), \tag{13}$$

$$\sigma_v^2 = u_*^2 \left(4.0 \left(1 - \frac{z}{h} \right)^{3/2} + 0.6 \left(-\frac{h}{L} \right)^{2/3} \right), \tag{14}$$

$$\sigma_w^2 = u_*^2 \left(1.7 \left(1 - \frac{z}{h} \right)^{3/2} + 3.3 \left(-\frac{z}{L} \right)^{2/3} \left(1 - 0.8 \frac{z}{h} \right)^2 \right). \tag{15}$$

Appendix 1.2: Turbulence Based on WRF Model Turbulent Kinetic Energy Field

In the second method for importing turbulence from the WRF model into the QUIC system, TKE fields are imported directly. As can be seen in the discussion above, the standard turbulence model in QUIC-PLUME is based on u_* instead of e. Unfortunately, the ability to export turbulence data from the WRF model is limited and does not provide a method to separate the 3D interpolated TKE field into the three velocity variance fields. WRF model TKE import scheme where the turbulence is based on the local e value rather than u_*. However, the random-walk dispersion model needs the velocity variances rather than e to determine

the turbulent diffusion within the plume. The definition of TKE (e) provides a relationship between TKE and the velocity variances but does not indicate the relative magnitudes of the velocity variances,

$$e = 0.5 \left(\sigma_u^2 + \sigma_v^2 + \sigma_w^2 \right). \tag{16}$$

For unstable conditions we can the combine the definition of e with Eqs. 13–15 to yield an equation for e as a function of u_*, z, h, and L,

$$e = u_*^2 \left(6.0 \left(1 - \frac{z}{h} \right)^{3/2} + 0.6 \left(-\frac{h}{L} \right)^{2/3} + 1.65 \left(-\frac{z}{L} \right)^{2/3} \left(1 - 0.8 \frac{z}{h} \right)^2 \right), \tag{17}$$

which can be rearranged to solve for u_*^2, which is then substituted back into Eqs. 13–15 to yield σ_u, σ_v, and σ_w in terms of e,

$$\sigma_u^2 = e \frac{f_1(z, h, L)}{f_0(z, h, L)}, \tag{18}$$

$$\sigma_v^2 = e \frac{f_2(z, h, L)}{f_0(z, h, L)}, \tag{19}$$

$$\sigma_w^2 = e \frac{f_3(z, h, L)}{f_0(z, h, L)}, \tag{20}$$

where f_0, f_1, f_2, and f_3 are the functions of z, h, and L within the parentheses on the right-hand side of of Eqs. 17, 13, 14, and 15, respectively. Similar substitutions can be made into Eqs. 10–12 for neutral and stable conditions, which become constant factors for the along-wind, cross-wind, and vertical components based on the standard relationships between u_* and σ values of the individual velocity components (Panofsky and Dutton 1984; Roth 2000). For the ratios of u_* and σ that the QUIC system uses, the ratios of velocity variances to e are 1.0, 0.67, and 0.28 for the along-wind, cross-wind, and vertical components, respectively.

References

Allwine KJ, Flaherty JE (2006) Joint urban 2003: Study overview and instrument locations. Tech. Rep. PNNL-15967, *PNNL*, Richland, Washington, USA, report available at https://ju2003-dpg.dpg.army.mil/

Allwine KJ, Leach MJ, Stockham LW, Shinn JS, Hosker RP, Bowers JF, Pace JC (2004) Overview of Joint Urban 2003 - an atmospheric dispersion study in Oklahoma City. In: Symposium on planning, nowcasting, and forecasting in the urban zone. American Meteorological Society, Seattle, WA, USA, p J7.1

Altman NS (1992) An introduction to kernel and nearest-neighbor nonparametric regression. Am Stat 46(3):175–185

Arya SP (1999) Air pollution meteorology and dispersion, 1st edn. Oxford University Press, New York, 310 pp

Arya SP (2001) Introduction to micrometeorology. International geophysics series, vol 79, 2nd edn. Academic Press, San Diego, 420 pp

Bentley JL (1975) Multidimensional binary search trees used for associative searching. Commun ACM 18(9):509–517

Brown MJ, Boswell D, Streit G, Nelson M, McPherson T, Hilton T, Pardyjak ER, Pol S, Ramamurthy P, Hansen B, Kastner-Klein P, Clark J, Moore A, Felton N, Strickland D, Brook D, Princevac M, Zajic D, Wayson R, MacDonald J, Fleming G, Storwold D (2004) Joint Urban 2003 street canyon experiment. In: Symposium on planning, nowcasting, and forecasting in the urban zone. American Meteorological Society, Seattle, WA, USA, p J7.3

Brown MJ, Zajic D, Gowardhan A, Nelson M (2008) Limits of fidelity in urban plume dispersion modeling: Sensitivities to the prevailing wind direction. In: 15th joint conference on the applications of air pollution meteorology with the AWMA. American Meteorological Society, New Orleans, LA, USA., p 6.1

Brown MJ, Gowardhan AA, Nelson MA, Williams MD, Pardyjak ER (2013) QUIC transport and dispersion modeling of two releases from the Joint Urban 2003 field experiment. Int J Environ Pollut 52(3–4):263–287

Burian S, Han W, Brown M (2003) Morphological analyses using 3D building databases: Oklahoma City, Oklahoma. Technical Report LA-UR-05-1821, LANL, Los Alamos, NM, USA

Calder KL (1966) Concerning the similarity theory of A. S. Monin and A. M. Obukhov for the turbulent structure of the thermally stratified surface layer of the atmosphere. Q J R Meteorol Soc 92:141–146

Chen F, Kusaka H, Bornstein R, Ching J, Grimmond CSB, Grossman-Clarke S, Loridan T, Manning KW, Martilli A, Miao S, Sailor D, Salamanca FP, Taha H, Tewari M, Wang X, A WA, Zhangh C (2011) The integrated wrf/urban modeling system: development, evaluation, and applications to urban environmental problems. Int J Climatol 31:273–288

Clawson KL, Carter RG, Lacroix DJ, Biltoft CA, Hukari NF, Johnson RC, Rich JD, Beard SA, Strong T (2005) Joint urban 2003 (ju03) sf6 atmospheric tracer field tests. Technical Report NOAA Technical Memorandum OAR ARL-254, NOAA, Field Research Laboratory, Idaho Falls, Idaho, USA

Coirier WJ, Kim S, Ericson SC, Marella S (2007) Calibration and use of site-specific urban weather observations data using microscale modeling. In: 14th symposium on meteorological observation and instrumentation. American Meteorological Society, San Antonio, TX, USA, p 5.4

Gowardhan AA, Pardyjak ER, Senocak I, Brown MJ (2011) A cfd-based wind solver for an urban fast response transport and dispersion model. Environ Fluid Mech 11(5):439–464

Hanna SR, Chang J (2012) Acceptance criteria for urban dispersion model evaluation. Meteorol Atmos Phys 116:133–146

Hanna SR, White J, Trolier J, Vernot R, Brown M, Gowardhan A, Kaplan H, Alexander Y, Moussafir J, Wang Y, Williamson C, Hannan J, Hendrick E (2011) Comparisons of JU2003 observations with four diagnostic urban wind flow and Lagrangian particle dispersion models. Atmos Environ 45(24):4073–4081

Hu XM, Nielsen-Gammon JW, Zhang Fa (2010) Evaluation of three planetary boundary layer schemes in the wrf model. J Appl Meteorol Clim 49:1831–1844

Kochanski A, Pardyjak E, Stoll JR, Gowardhan A, Brown MJ, Steenburg WJ (2015) One-way coupling of the wrfquic urban dispersion modeling system. J Appl Meteorol Clim 54(10):2119–2139

Lin CY, Chen F, Huang JC, Chen WC, Liou YA, Chen WN, Liu SC (2008) Urban heat island effect and its impact on boundary layer development and land sea circulation over northern Taiwan. Atmos Environ 42:5635–5649

Liu Y, Chen F, Warner T, Basara J (2006) Verification of a mesoscale data-assimilation and forecasting system for the Oklahoma City area during the Joint Urban 2003 field project. J Appl Meteorol Clim 45:912–929

Lundquist KA, Chow FK, Lundquist JK (2012) An immersed boundary method enabling large-eddy simulations of flow over complex terrain in the WRF model. Mon Weather Rev 140:3936–3955

Monin AS, Obukhov AM (1954) Basic laws of turbulent mixing in the ground layer of the atmosphere. Trudy Geophys Inst ANSSSR 151(24):163–187

Nelson MA (2014) Building effects on plume residence time. In: Chemical and biological warfare weaponization and consequence assessment modeling symposium. National Ground Intelligence Center, Charlottesville, VA, USA

Nelson MA, Pardyjak ER, Klewicki JC, Pol SU, Brown MJ (2007) Properties of the wind field within the Oklahoma City Park Avenue street canyon. Part I: Mean flow and turbulence statistics. J Appl Meteorol Clim 46:2038–2054

Nelson MA, Williams MD, Zajic D, Pardyjak ER, Brown MJ (2009) Evaluation of an urban vegetative canopy scheme and impact on plume dispersion. In: 8th symposium on the urban environment. American Meteorological Society, Phoenix, AZ, USA, p JP6.4

Nelson MA, Brown MJ, Halverson SA, Bieringer P, Annunzio A, Bieberbach G, Meech S (2016) A case study of the weather research and forecasting model applied to the joint urban 2003 tracer field experiment. part 1: Wind and turbulence. Boundary-Layer Meteorol 158(2):285–309

Neophytou M, Gowardhan A, Brown M (2011) An inter-comparison of three urban wind models using Oklahoma City Joint Urban 2003 wind field measurements. J Wind Eng Ind Aerodyn 99:357–368

Panofsky HA, Dutton JA (1984) Atmospheric turbulence. Wiley, New York, 424 pp

Pardyjak ER, Booth TM, Brown MJ (2004) A simple data assimilation technique for a fast response urban wind model. In: Fifth conference on urban environment. American Meteorological Society, Vancouver, BC, Canada, p 6.9

Pasquill F, Smith FB (1984) Atmospheric diffusion, 3rd edn. Wiley, New York, 429 pp

Röckle R (1990) Bestimmung der stomungsverhaltnisse im bereich komplexer bebauungsstrukturen. PhD thesis, Vom Fachbereich Machanik, der Technischen Hochshule, Darmstadt, Germany

Rodean HC (1996) Stochastic Lagrangian models of turbulent diffusion. American Meteorological Society, Boston

Rodriguez LM, Bieringer PE, Warner T (2013) Urban transport and dispersion model sensitivity to wind direction uncertainty and source location. Atmos Environ 64:25–39

Roth M (2000) Review of atmospheric turbulence over cities. Q J R Meteorol Soc 126:941–990

Skamarock WC, Klemp JB, Dudhia J, Gill DO, Barker DM, Wang W, Powers JG (2005) A description of the advanced research wrf version 2. Technical Report NCAR/TN468+STR, NCAR

Stull RB (1988) An introduction to boundary layer meteorology. Kluwer Academic Publishers, Dordrecht, 670 pp

Tewari M, Kusaka H, Chen F, Coirier WJ, Kim S, Wyszogrodzki AA, Warner TT (2010) Impact of coupling a microscale computational fluid dynamics model with a mesoscale model on urban scale contaminant transport and dispersion. Atmos Res 96:656–664

Wang W, Bruyre C, Duda M, Dudhia J, Gill D, Kavulich M, Keene K, Lin HC, Michalakes J, Rizvi S, Zhang X, Beezley JD, Coen JL, Mandel J, Chuang HY, McKee N, Slovacek T, Wolff J (2015) Weather research and forecasting ARW version 3 modeling system user guide. http://www2.mmm.ucar.edu/wrf/users/docs/user_guide_V3/contents.html. Accessed: 3 Dec 2015

Warner TT, Benda P, Swerdlin S, Knievel J, Argenta E, Aronian B, Balsley B, Bowers J, Carter R, Clark P, Clawson K, Copeland J, Crook A, Frehlich R, Jensen M, Liu Y, Mayor S, Meillier BY abd Morley, Sharman R (2007) The Pentagon Shield field experiment: toward protecting national assets. Bull Am Meteorol Soc 88:167–176

Williams MD, Brown MJ, Singh B, Boswell D (2004) Quic-plume theory guide. Technical Report LA-UR-04-0561, LANL, Los Alamos, NM, USA

Wyszogrodzki AA, Miao S, Chen F (2012) Evaluation of the coupling between mesoscale-wrf and leseulag models for simulating fine-scale urban dispersion. Atmos Res 118:324–345

Xie B, Fung JCH, Chan A, Lau A (2012) Evaluation of nonlocal and local planetary boundary layer schemes in the WRF model. J Geophys Res 117(D12):103